Alternatives for upgrading the EU DCLL breeding blanket from MMS to SMS

Iván Fernández-Berceruelo[1], Iole Palermo[1], Fernando R. Urgorri[1], Ángela García[1], David Rapisarda[1], Luis Moya[2], Fernando Rueda[2], David Alonso[2] and Ángel Ibarra[1]

[1] *Fusion National Laboratory, CIEMAT, Avda. Complutense 40, 28040 Madrid, Spain*
[2] *ESTEYCO, S.A., Calle Menéndez Pidal 17, 28036 Madrid, Spain*

In the last years, CIEMAT worked in the development of a low temperature DCLL breeding blanket design aimed at using conventional materials and technologies. It followed the multi-module segment (MMS) approach, which allows operating within the thermal range tolerated by EUROFER while keeping a low bulk velocity of the self-cooled liquid breeder (PbLi) in the breeding zone. Thinking in the commercial exploitation of fusion, it must be taken into account that there is risk that the foreseen availability goal in fusion reactors is not achieved. In that case, the limited net efficiency of low temperature blankets could not be sufficient to obtain a competitive cost of the electricity. For that reason, more advanced blanket solutions are being explored with the objective of developing a simpler, more reliable and more efficient design based on a single-module segment (SMS) architecture and the use of self-cooled incompressible liquid breeder. In this work, different strategies to solve interrelated aspects like the topology and electrical insulation of the breeder circuits, the first wall integration and the main neutronic responses are analysed and discussed.

Keywords: DEMO, DCLL, blanket.

1. Introduction

CIEMAT worked along several years in the design of a breeding blanket (BB) based on the dual-coolant lithium-lead (DCLL) concept [1]-[3], in which PbLi acts as main coolant, tritium breeder, tritium carrier and neutron multiplier while helium cools the first wall and other structures. The European DEMO Programme encouraged the development of a "low temperature" version of the DCLL BB to allow using conventional materials and technologies. This approach led to adopt the multi-module segment architecture (MMS), in which the blanket is split into a number of vertical segments, and each segment is composed, in turn, by a series of modules attached to a common back supporting structure (BSS) which also accomplishes functions of manifold and shield (Fig. 1). The arrangement of individual fluid circuits in parallel made possible to operate within the thermal range tolerated by EUROFER (300-550°C) while keeping the bulk velocity of the self-cooled liquid breeder as low as ~2 cm/s in the breeding zone, which involves important benefits from the point of view of magnetohydrodynamics (MHD) and corrosion. The design also included flow channel inserts (FCI) to electrically decouple the liquid metal bulk flow from the steel walls.

Paving the way from demonstration reactors towards power plants, economic studies consider that the cost of electricity generated by fusion will be dominated by capital construction cost rather than operating cost, so that plant availability will be a more important factor than in other generation technologies [4]. The efficiency of the power conversion cycle will be another decisive parameter to establish the cost of electricity. What is not proven is that the assumed power levels, conversion efficiency and most notably availability can be achieved in practice [5]. Therefore, there is a risk that the limited net efficiency of low temperature blankets is not sufficient to obtain a competitive cost of electricity generated by fusion. For that reason, more advanced blanket solutions are being explored with the objective of developing simpler, more reliable and more efficient designs. Key aspects to achieve such goal are the use of a self-cooled incompressible liquid breeder, which is a vector to high efficiencies, and segments with single module segment architecture (SMS), which can help in providing more simplicity and reliability.

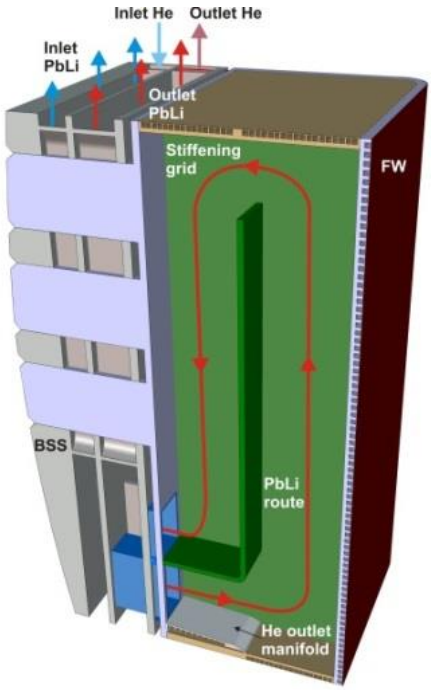

Fig. 1. DCLL MMS design (2014-2018). PbLi/He main routes in the module located at the OB equatorial level.

author's email: ivan.fernandez@ciemat.es

The strategy proposed here consists in a deep evolution of the DCLL concept in aspects like structural material, electrical insulation method, topology of the fluid circuits and first wall (FW) integration. Different alternatives for each of those aspects have been considered and certain design or technology options have been preliminarily selected for further assessment. The reasons which justify such choices are discussed in Section 2. Additionally, Sections 3-8 are devoted to describe some specific calculations (MHD, neutronics, thermomechanics, etc.) in support of them.

2. Discussion of alternatives

2.1 Structural material and electrical insulation method

Option 1: Advanced steel + coating. Oxide dispersion strengthened (ODS) EUROFER is perhaps the most attractive option as structural material for a moderate increase of the operational temperature because of its good tensile and creep properties, which would allow operating at T~650ºC [6]. However, its corrosion behaviour is not much better than the EUROFER97 one. This can be solved by applying a coating on the surface of the PbLi channels which acts as corrosion barrier and electrical insulator. The main disadvantage is that this solution depends on the development of both technologies (ODS EUROFER and coatings) beyond the current state-of-the-art. For example, hot isostatic pressure (HIP) is practically the unique joining technology that can be employed with ODS EUROFER at present. Furthermore, its cost is much higher than the EUROFER97 one. For these reasons, reduced activation ferritic-martensitic (RAFM) steels for high temperature applications seem to be a more viable alternative. Special thermomechanical treatments (TMT) and fine-tuning of the chemical composition can improve high temperature strength, creep and creep fatigue properties of 9%Cr RAFM steels and consequently expand their thermal operation window [7].

With respect to coatings, Al_2O_3 nanoceramic coatings grown by pulsed laser deposition (PLD) [8] have obtained very promising results in terms of i.e. mechanical performance, electrical resistivity, permeation reduction ratio and corrosion against static PbLi at 550ºC. Nevertheless, the technique has not been demonstrated to work on wide areas and non-planar surfaces.

Option 2: EUROFER + FCI (including thermal insulation). As in the case of the EU MMS DCLL design, a common approach for high temperature DCLL blankets in different R&D programmes [9] has been the use of RAFM steel as structural material and FCIs to electrically decouple the PbLi bulk flow and the walls. But in these cases the FCIs must also provide thermal insulation between the PbLi bulk (T up to 700ºC) and the walls, which should be kept under T=550ºC. The presence of the FCIs makes necessary to cool the Hartmann walls (perpendicular to the magnetic field), where the PbLi which fills the gap between the FCI and the walls is almost stagnant [10]. This leads to He circuits longer and more complicated (higher pressure drop), which increases the ratio of power extracted by He with respect to PbLi and has unfavourable effects on the net efficiency of the power conversion system. On the contrary, PbLi velocity jets are expected to appear next to the side walls (parallel to the magnetic field) and magnify the local corrosion rate. Additionally, due to different thermal expansion coefficients of ceramic and RAFM steels, high thermal stresses can appear in the case of sandwich-type FCIs [11], seriously compromising the integrity of the component.

Option 3: ceramic box containing the breeding zone. The idea is to use an electrically resistive and PbLi-compatible ceramic or ceramic matrix composite (CMC) as structural material for the breeding zone. This line entails relevant challenges linked to the behaviour of brittle materials and the possible occurrence of swelling, and obliges to develop ceramic-metallic pipe connections. Furthermore, there are not many ceramics that combine good mechanical and electrical properties with a desirable low-activation behaviour. In fact, different radiological magnitudes (specific activity, decay heat and contact dose rate) of a number of technical ceramics have been studied in this work by means of activation calculations to characterize them in terms of kind of maintenance operations and waste management. The neutronic model of the former MMS design [3] with modified material compositions has been employed. The transport calculations have been performed using Monte Carlo code MCNP5 [12] and JEFF3.1.1 XS data library [13]. The activation responses have been determined by using the ACAB inventory code [14] and the nuclear data library EAF2007 [15]. The results have been classified in three categories according to three different regulations: IAEA, SEAFP-2 and the one specific from the near-surface repository El Cabril (Córdoba, Spain). None of the compositions evaluated are fully compliant with the low level waste (LLW) and short lived waste limits (Table 1). SiC and TiC are the most favourable ones. Among them, TiC can be discarded by its low electrical resistivity.

Table 1. Colour classification of the assessed ceramics according to different activation aspects (DH: decay heat, CDR: contact dose rate, ACT: specific activity). Green means compliance with the LLW and short lived waste limits.

	Al_2O_3	**SiC**	**ZrO_2**	**Si_3N_4**
DH				
CDR				
ACT				
	ZrC	**TiZrC**	**TiB_2**	**$TiZrB_2$**
DH				
CDR				
ACT				
	AlON	**Fused SiO_2**	**AlN**	**Mullite**
DH				
CDR				
ACT				
	TiC	**$MgAl_2O_4$**	**MACOR**	**EUROFER**
DH				

Despite the mentioned issues, the ceramic box solution permits surpassing the limit in the operational temperature imposed by creep in RAFM steels, as well as simplifying the breeding zone by suppressing the need of FCIs. Another advantage is the reduction of electromagnetic loads acting on the structure. Finally, it can benefit from the experience in ceramics R&D gained from FCIs. Taking into account the previous points, it has been decided to explore this option in first place. The advanced steel + coating option, and to a lesser degree the EUROFER + FCI option, are kept as backup solutions.

2.2 First wall-breeding zone integration

Although the breeding zone walls are made of ceramic, an alloy must be employed to manufacture the FW since, at present, it is not possible to obtain the required tolerances in the manufacturing of large ceramic components pierced by cooling channels with thin walls. Furthermore, the very limited ability of ceramics to redistribute stress, as a result of their low ductility, makes them inadequate to deal with thermal stress concentrations originated by pronounced heat flux peaks. Thus, two options to integrate the FW and the breeding zone have been initially examined:

Option 1: detached FW modules. This approach consists in a FW hydraulically and mechanically detached from the rest of the blanket (e.g. fingers) which covers the front side of the breeding zone. It involves several problems. Firstly, the ceramic structure would not be completely enclosed by the FW panel, so PbLi could be spilt into the vacuum vessel in case of structural failure of the brittle holder. Secondly, the integration of the FW manifolds and mainly the assembly/disassembly by remote handling are not solved yet.

Option 2: enveloping steel case. The ceramic box which encloses the breeder circuit is protected by a EUROFER steel case including a continuous FW panel. Both are separated as much as possible to accommodate the different thermal expansion of dissimilar materials. This also allows establishing two thermal levels: 300-550ºC for the steel case and 300-700ºC for the ceramic box. If the steel case is hermetic, the gap with the ceramic box should be filled by a low pressure inert gas (e.g. He or Ar) flowing at low velocity in order to drag gaseous activation products and help to smooth hot spots. Since it does not accomplish cooling functions, the necessary circulation power should be very low. The main issues of this option are the design of the interface between the ceramic box and the steel case, the addition of the filling gas circuit and the impact of the double wall (alloy + ceramic) on tritium production. Sections 6, 7 and 8 are respectively dedicated to them. In any case, this option is preferable from the points of view of safety and integrability and it has been selected for further studies.

2.3 Plasma facing material and first wall cooling

Option 1: adaptation of liquid metal divertor concepts for the FW. Capillary porous systems (CPS) are a representative example. They are based on the wettability of Li or Sn, low Z elements which present some advantages over W as plasma facing materials and make possible to exploit phase change for cooling. This is a very interesting approach to explore in the short term, although its design and integration with the rest of the BB requires a deep evaluation. Moreover, there are a number of uncertainties concerning its functioning.

Option 2: W + RAFM steel. This has been the baseline approach through different DEMO programmes. In the case of the EU DEMO, it consists in a layer of W of 2 mm thickness joined to a EUROFER structure, which is cooled by a succession of toroidal channels with small cross-section area. During the last years, a great deal of effort has been put in R&D activities focused on solving problems related to this configuration (manufacturing techniques, heat transfer enhancement, wall protection, etc.). Taking into account its higher level of development, it has been selected as reference in this work. Regarding the coolant, some of the fluids previously proposed in the field of fusion technology can be examined. PbLi is not a suitable coolant for the FW since it should flow at very high velocity to effectively cool zones subjected to heat fluxes up to ~1.3 MW/m^2 and it is not feasible to provide electrical insulation to the whole set of channels. Some molten salts, like FLiBe or ClLiPb, have the advantage of low electrical conductivity, so that no additional insulating methods should be required. However, they present some drawbacks: incompatibility issues with steels, chemical control of the molten salt during irradiation, high melting temperature, low thermal conductivity, etc. H_2O has excellent properties as coolant but i.e. pressurized-water reactor (PWR) conditions are hardly compatible with the thermal level foreseen in the ceramic box. Helium combines adequate thermophysical properties and safety characteristics. For this reason, it has been selected in this work, like in other DCLL designs. Section 3 is dedicated to model the functioning of the FW cooling system. Nevertheless, it is worth noting that He is a light and compressible fluid whose need of recompression power to compensate pressure loss along the circuit is much larger than the pumping power required for incompressible fluids like liquid metals. It must be also underlined that He is expensive, scarce and, fundamentally, susceptible to leak. In an industrial-scale facility like DEMO or a power plant with kilometres of fluids transport lines, controlling a great number of small leaks could be a serious problem. CO_2 is a heavier gas with larger size molecules which has been already proposed in previous works as an alternative for He-cooled blankets, i.e. [16], although it is necessary to clarify possible radiological issues. The cooling performance of He and CO_2 for the SMS DCLL FW is compared in Section 4.

2.4 Topology of the PbLi circuits

Option 1: parallel poloidal channels. It is the classical topology of liquid metal circuits in different concepts of high velocity BB [9][17]. Such configuration ensures a flow path as simple as possible which minimizes MHD pressure drop associated to 3D geometrical features, whereas pressure drop due to electrical coupling between PbLi and walls is expected to be mitigated by insulating elements (FCIs, coatings, intrinsic electrical conductivity of the walls, etc.).

Option 2: B-oriented channels. Although the poloidal component of the magnetic field is frequently disregarded in calculations, it is certainly significant in comparison with the toroidal one. In fact, in DEMO 2017 [18] the resultant vector forms an angle of 6-15º with respect to the horizontal plane. If the PbLi channels are oriented in the same direction of the magnetic field, the 2D fraction of the MHD pressure drop (the one associated to cross-sectional currents) is cancelled. Of course, a helicoidal flow path is not compatible with the current blanket architecture, which has been set according to requirements of vertical maintenance. However, it is possible to introduce bends to confine the liquid metal circuit inside the characteristic toroidal size (ζ) of a blanket segment so that most of the path PbLi follows the magnetic field direction (Fig. 2). The question is how much important is the 3D pressure drop associated to the bends in comparison with the annulled two-dimensional fraction.

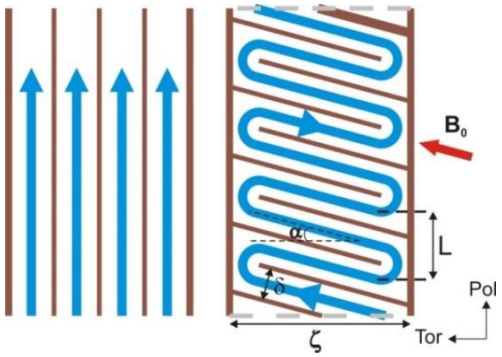

Fig. 2. Options 1 (left) and 2 (right) for the topology of the PbLi circuits.

Section 5 is focused on the numerical comparison of both options from the point of view of MHD pressure drop. As it is demonstrated there, the B-oriented configuration, with both conductive and insulated walls, does not provide better MHD performance than the classical configuration in DEMO conditions.

Once selected the configuration of poloidal channels, it must be taken into account the need of stiffening the breeding zone structure by a flow divisor which radially separates the PbLi circuit in two parts. Thus, the relationship between the flow direction in both the front and rear channels is also relevant. Two possibilities have been set out:

Option 1a: antiparallel channels. The common antiparallel circulation in poloidal PbLi channels (upwards in the front channels and subsequent downwards in the rear ones, Fig. 1) is problematic due to the MHD-buoyancy interaction [19]. Indeed, hot spots and He bubbles nucleation, growth and trapping could occur in the low velocity zone created near the top 180º bend. In addition, a descending jet could appear in the rear channels next to the dividing stiffener, which would lead to excessive corrosion rates.

Option 1b: parallel channels. Upwards circulation in both front and rear channels is able to suppress both problems. However, due to radial differences in nuclear heating, higher velocity is required in the front channels. MHD makes difficult to achieve a convenient flow distribution inside the blanket. For that reason, it is proposed to use independent feeding pipes for the front and rear channels, respectively (Fig. 3). The choice of the parallel circulation and the specification of the outlet temperature in 700ºC are able to keep the average PbLi velocity in the front channels as low as 6-7 cm/s.

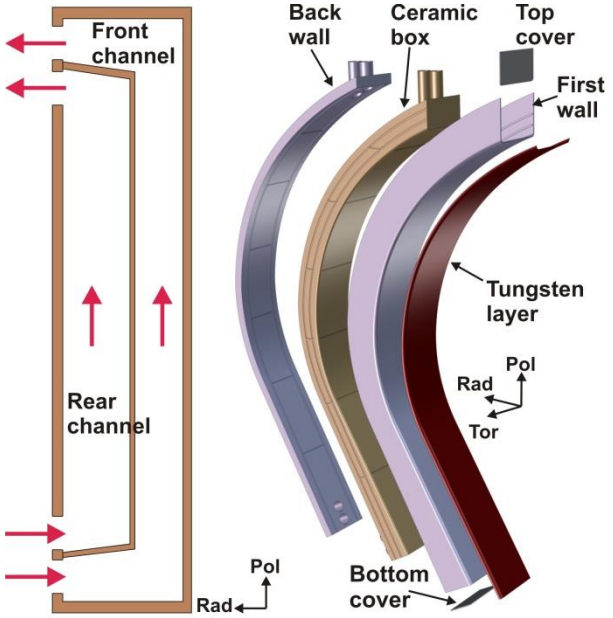

Fig. 3. PbLi circulation scheme (left). Exploded view of the OBC segment components (right) (He pipes not shown).

2.5 Ceramic box-steel case interfaces

One of the most critical issues of this concept of high temperature blanket is the arrangement of the interfaces between the ceramic box (breeding zone) and the steel envelope (FW). Indeed, it is not easy to envisage supporting solutions which keep equilibrium between robustness and freedom. Several possibilities have been examined.

Option 1: suspension approach. It is based on the combination of springs, shock absorbers and linkages to keep together both sides of the interface and absorb relative movement between them. Although elements capable of storing elastic potential energy can provide the required flexibility and strength, they are susceptible to suffer stress relaxation and creep by irradiation.

Option 2: shear keys + additional gravity supports. This proposal has been selected for the initial design of the blanket (Fig. 3). The objective is to transmit efforts

between the ceramic box and the steel envelope, avoiding relative rotations. As shown in Section 6, this solution is effective to decouple the deformation of the ceramic and steel components. Nevertheless, it has been verified that it depends excessively on the accurate prediction of the whole structure deformed shape.

Option 3: hinged support + roller support (Fig. 4). The key concept is to simplify the connection scheme between the ceramic box and the steel envelope as far as possible to thermally decouple both components. The isostatic support condition devised results in a robust design and avoids undesired and hardly predictable stress concentrations in the ceramic owing to differential thermal expansions during operation. The load transfer is proposed to be realized through metallic elements inserted into the ceramic.

A preliminary numerical evaluation of this proposal indicates that it can provide a very good performance against a loading of temperature, weight and hydrostatic pressure which much less sensitivity to the characteristics of the overall deformation [20]. Therefore, it is proposed to further develop this line.

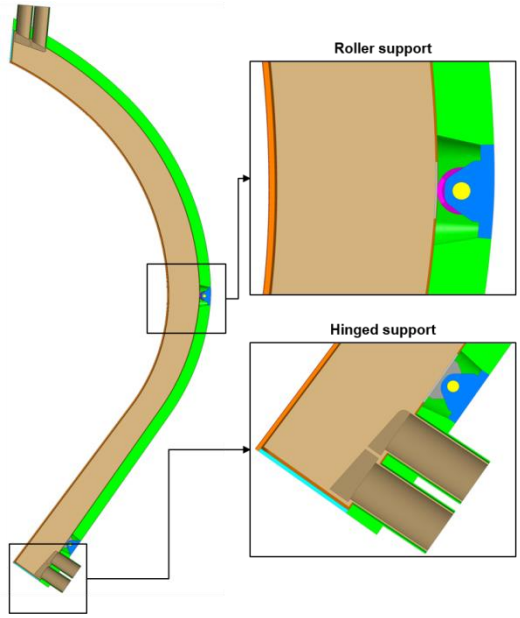

Fig. 4. Hinged support + roller support conceptual design.

3. Coolability of the FW

The irregular spatial distribution of heat flux on the FW due to radiation from the plasma and charged particles is undoubtedly challenging for the design of the FW cooling system. Indeed, a conservative oversizing of the coolant mass flow rate can have a severe impact on the blanket thermal efficiency and the consumption of the auxiliary systems, since He is employed –together with PbLi- as thermal source for the power conversion system (it represents ~30% of the power extracted from the blanket). For that reason, it is convenient to find a methodology which allows studying the manageability of adjusting mass flow rates in individual FW channels to local cooling requirements. A computational fluid dynamics (CFD) model of the entire FW with conjugate heat transfer is too demanding from the point of view of computational resources. Nevertheless, it is feasible to study the coolability of the whole component by means of simplified thermal-hydraulic finite element analyses (FEA). The solid bodies can be modelled by layered shell-type elements with temperature variation through layer (in-plane and through-thickness thermal conduction capability). Coupled thermal-fluid pipe elements can represent the fluid streams, with temperature and pressure as degrees of freedom (DOF). Finally, these can be connected to shell-type elements through thermal surface elements in order to model convective heat transfer. This methodology has been followed here to create a model of the outboard central segment (OBC) in ANSYS APDL.

The model geometry includes the front and radial walls of the OBC steel envelope (U-shape, Fig. 3). The top/bottom temperature DOF of the coincident nodes belonging to the W layer and the EUROFER front shell are coupled to simulate heat conduction through the interface. Independently fed helium streams in counterflow are represented by linear elements with square cross section. The whole numerical model is composed by 3.66 M elements. Regarding loads and boundary conditions, the heat flux distribution calculated for DEMO 2017 [21] has been mapped onto the W external surface. Nuclear heating in W and EUROFER is also included. He bulk temperatures and heat transfer coefficients are calculated for each fluid/thermal surface element, respectively, during the solving process by applying Gnielinski's correlation [22]. An inlet temperature of 300ºC has been considered for every channel, which means disregarding heat transfer along the manifolds. Finally, the surfaces facing the gap are considered adiabatic. EUROFER, He and W properties have been taken from [23], [24] and [25], respectively.

Prior to solving, several subroutines are used to couple the ANSYS APDL model with the system level code PLATOON [2] in order to estimate the mass flow rate for each of the 817 He channels of the OBC FW required to keep the EUROFER part under 550ºC. This approach uses the magnitude and position of the local peak values of heat flux in relation with the He flow direction (from left to right or vice versa). The results have demonstrated that the methodology is sufficiently accurate for a preliminary appraisal of the cooling needs (Fig. 5).

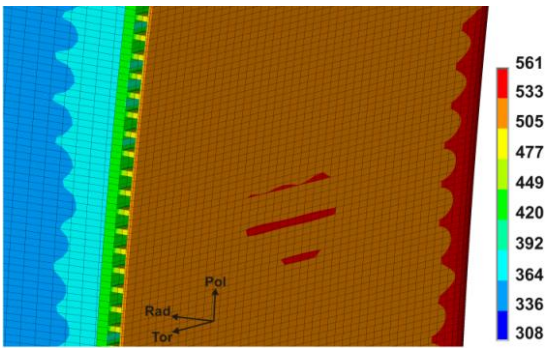

Fig. 5. Temperature contours (ºC) in a section of the OBC FW (thickness shown).

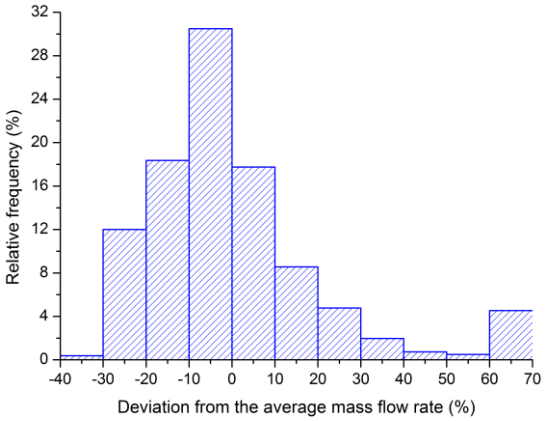

Fig. 6. Histogram of the deviation from the average mass flow rate in the OBC FW channels.

The total mass flow rate (14.7 kg/s), calculated from the sum of individual mass flow rates, is 25% lower than the corresponding to the channel where the absolute peak value of heat flux in the whole FW occurs multiplied by the total number of channels. The difference is important, although the conservative approach could be a suitable solution for the OBC. Indeed, achieving a good flow distribution with a tapered Z-manifold is reasonably straightforward. But it can be significantly more challenging if individual flow rates are adapted to the local heat loads (Fig. 6). In the case of the outboard lateral segments and especially the inboard (IB) segments the differences between peak and average heat flux values are much more noticeable and heterogeneous mass flow rates are mandatory to avoid jeopardizing the balance of plant. Variable wall roughness and channel sizes, as well as heat transfer enhancement structures are among the most reliable methods to modify the flow distribution. The next step is to upgrade the model with a common inlet and outlet, tapered manifolds and fluid dynamics features (friction factors depending on roughness, loss coefficients, etc.) which allow evaluating to what extent it is possible to reproduce the optimal mass flow rates calculated in independent channels.

4. CO_2 as alternative FW coolant

3D CFD steady-state analyses with conjugate heat transfer have been carried out in ANSYS Fluent to compare the performance of He and CO_2 as coolant for the FW. The model takes advantage of the linear periodic symmetry of the OBC FW cooling system along the poloidal direction. Therefore, it only includes two coolant streams in counterflow and the corresponding W and EUROFER parts. Smooth channels of 12.5 x 12.5 mm^2 have been considered, with a pitch of 5 mm and a front wall thickness of 2 mm. Constant thermophysical properties at 8 MPa and 300ºC have been used for both fluids, excepting the temperature-dependent density (described by piecewise linear functions) [24]. The properties of EUROFER and W have been taken from [23] and [25], respectively. Nuclear heating in both W and EUROFER has been evaluated, as well as two levels of uniform heat flux on the W surface (0.2 and 0.6 MW/m^2). K-ω SST has been employed as turbulence model. Apart from periodicity, inlet velocity (T=300ºC) and null gauge pressure in the outlet have been imposed as boundary conditions. In addition, the surfaces facing the gap are considered adiabatic.

A range of inlet velocities has been swept for each heat flux and coolant, with the aim of obtaining the minimum required to keep EUROFER temperature under 550ºC. Table 2 exposes the main outcomes of the assessment. Q is the volumetric flow rate, T_{outlet} is the He temperature at the outlet, η_c stands for Carnot's cycle efficiency, Δp is the pressure loss, P_{recomp} is the recompression power (electrical power needed to recompress the coolant at the reference pressure) and η_{recomp} is the so called recompression efficiency.

$$\eta_c = 1 - \frac{\overline{T_{sink}}}{\overline{T_{coolant}}} \quad (1)$$

$$P_{recomp} = \frac{1}{\eta_{circ}} \cdot \frac{\gamma}{\gamma - 1} \cdot Q \cdot P_1 \cdot \left(\frac{P_2}{P_1}\right)^{\frac{\gamma-1}{\gamma}-1} \quad (2)$$

$$\eta_{recomp} = 1 - \frac{P_{th}}{P_{recomp}} \quad (3)$$

Where T_{sink} and $T_{coolant}$ are the logarithmic mean temperature differences in the sink and the coolant, respectively. Values of 298 and 303 K have been assumed, respectively, for the inlet and the outlet temperatures in the sink [26]. γ is the heat capacity ratio, P_2 is the reference operating pressure (80 bar), P_1 is obtained by subtracting the pressure loss to P_2, η_{circ} is the circulator isentropic efficiency (a value of 0.82 has been assumed here [26]) and P_{th} is the thermal power extracted by the coolant.

As can be seen, the performance of CO_2 is slightly poorer, but it could be a potential substitute for He if it is proven that it does not present major radiological issues.

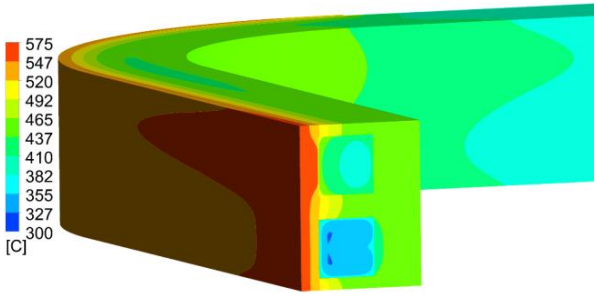

Fig. 7. Temperature contours in a sector of the FW periodic model (case with CO_2, 0.2 MW/m^2 and v_{inlet}=7 m/s).

Table 2. Comparison between He and CO_2 for the inlet velocity needed to keep the EUROFER part of the FW under 550ºC.

	0.2 MW/m²		0.6 MW/m²	
	He	CO_2	He	CO_2
v (m/s)	17.29	7.78	56.43	30.25
Q (m³/s)	2.207	0.994	7.203	3.862
T_{outlet} (ºC)	412.5	400.6	374.7	355.8
η_c (%)	52.1	51.7	50.7	50.0
Δp (Pa)	5402	8905	43817	95025
P_{recomp} (W)	14535	10785	384286	445428
η_{recomp} (%)	99.83	99.87	97.92	97.59

5. PbLi poloidal channels vs B-oriented channels

This Section explains the methodology to compare the 3D pressure drop associated to the bends in the B-oriented configuration and the annulled 2D fraction, as introduced in Subsection 2.4. In order to establish a comparison criterion, it must be taken into account that the increase of temperature per unit of PbLi volume and poloidal length should be the same in both schemes. This implies that the ratio of mean velocities in the classical (poloidal channels) and alternative (B-oriented channels) configurations must be equal to the ratio between the channel height (δ) and the segment toroidal dimension (ζ) (Fig. 2):

$$\frac{u_{cl}}{u_{alt}} = \frac{\delta}{\zeta} \tag{4}$$

Following this restriction, the criterion selected here to compare the pressure drop produced in the classical and alternative paths is the so called 3D equivalent length (d_L), defined as follows [27]:

$$d_L = \frac{\Delta p_{3D}}{\delta_L p_{2D}} \tag{5}$$

Physically, it can be interpreted as the poloidal distance covered by PbLi in the alternative configuration which produces the same pressure drop necessary to raise PbLi a fixed length (L) in the classical configuration. Therefore, the alternative configuration will be competitive just in case d_L is lower than L. The pressure drop in the classical configuration has been calculated using a correlation for insulated [28] and conductive walls [29], respectively. MHD numerical simulations have been carried out using ANSYS Fluent to calculate the 3D pressure drop associated to the turns of the alternative configuration under different combinations of Hartmann and Reynolds numbers. Two cases have been evaluated: with perfectly insulated walls and with conductive walls of 15 mm thickness. The input parameters are exposed in Table 3. Constant thermophysical properties of PbLi at 550ºC [30] and EUROFER at 500ºC [23] have been utilized.

The 3D MHD results show that currents induced the plane coincident with the baffle plate produce strong Lorentz forces in the vicinity of the turn (Fig. 8, right), causing the expected 3D pressure drop. Velocity deviates close to the walls where the currents are locally parallel to the field (Fig. 8, left). Next to tip of the baffle plate the MHD forces produce a counterflow bubble. In the case of insulating walls, the already reduced 2D pressure drop of the classical configuration is much lower than the 3D contribution of the alternative one. Therefore, the alternative configuration is not competitive in any case.

Table 3. Input parameters for the MHD simulations.

Poloidal channels	2a (m)	0.3
	2b (m)	0.3
	u_p (cm/s)	6.5
B-oriented channels	δ (m)	0.3
	ζ (m)	0.7 / 0.5 / 0.3
	α (º)	15
	$u_{b\text{-}or}$ (cm/s)	15.2 / 10.8 /6.5

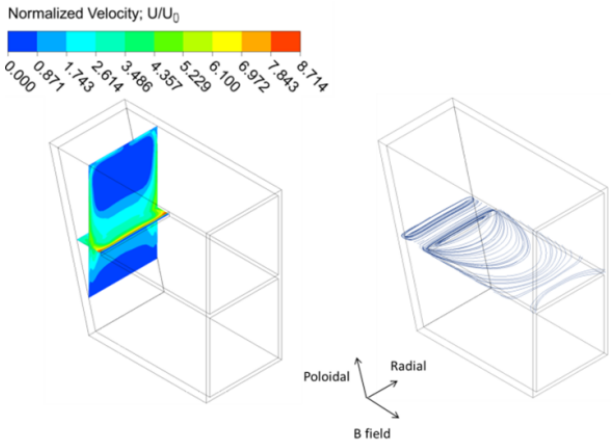

Fig. 8. Velocity distribution next to the turn (left) and induced currents in the field-radial plane (right) in the case of the conducting walls and Ha=2000.

From the results of 8 simulations it has been possible to find a good 2-dimensional fitting (R^2=0.9995) of the equivalent length with Reynolds and Hartmann numbers for the conductive walls case:

$$d_L(Ha, Re) = 1.72 \cdot 10^{-4} Ha^{-0.87} \cdot Re^{1.45} \tag{6}$$

Since the values of α and δ have been fixed, the limit value of the equivalent length for the alternative configuration is ~0.621 m. As anticipated in Section 2, DEMO conditions (Ha~10^4, Re~$2 \cdot 10^5$) lead to higher equivalent lengths, so the B-oriented channels with conductive walls are neither a practical alternative to the classical poloidal channels. The B-oriented channels without insulation might just present some benefits with low fluid velocities and high magnetic field.

6. Performance of a supporting system based on shear keys

The functioning of the shear keys system (option 2 in Subsection 2.5) can be illustrated by means of a quite simple 2D steady-state FEA. The model geometry (Fig. 9), adapted from the equatorial section of the OBC segment, is composed by the ceramic box (grid of 6 parallel circuits formed by poloidal channels), the steel case and the back wall (both solid). All the walls have a thickness of 25 mm excepting the back wall (250 mm). In this case, alumina has been considered as testing

material for the ceramic box [31] because of the previous experience in the manufacturing of FCIs, although the results can be applicable to some other ceramic materials.

The interfaces between the alumina and EUROFER bodies around the shear keys have been modelled by frictional contacts (0.2 as friction coefficient), which are initially open according to the detailed views A and B in Fig. 9. Two load steps (consecutive and additive) have been considered: 1) heating from room temperature to uniform values of 700 and 400ºC in the ceramic box and steel parts, respectively; and 2) combination of a characteristic electromagnetic resultant force (F_{rad}=-$2.125 \cdot 10^5$ N; F_{tor}=-606.8 N) and a moment (M_{pol}=$1.2 \cdot 10^4$ Nm) has been applied, divided among the whole set of nodes. Neither own weight nor PbLi hydrostatic pressure has been considered in this 2D model, although the combination of both loads has certain relevance in the bottom part of the segment [32].

During both load steps, null displacement has been set in two nodes located at the rear side of the BW (Fig. 9). Additionally, two slender beams avoid rigid body motion in the ceramic box.

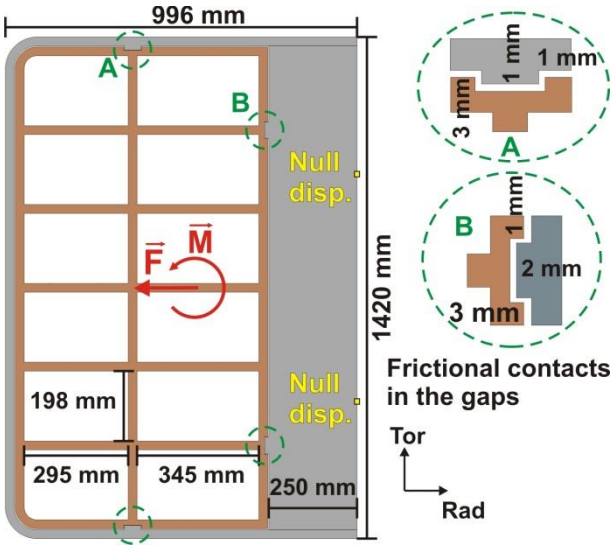

Fig. 9. Main dimensions and boundary conditions in the 2D finite element model.

The higher thermal expansion of EUROFER compensates the lower operational temperature, so the maximum displacements in both materials are quite similar at the end of the 1st load step. However, the boundary conditions at the rear of the back wall and the greater freedom of the ceramic box to expand provoke the closing of the contacts while the stress level is kept low. During the application of the 2nd time step, the closed contacts prevent a larger radial displacement of the box and a general rotation without increasing significantly the overall stress level (average values of the 1st principal stress around 3-5 MPa).

It results of interest to verify the integrity of the structure according to a statistical criterion [32]. In brittle materials, strength depends on the size of the largest (or critical) defect in a specimen, and this can differ from component to component. Therefore, a strength distribution function is necessary [33]. The well-known Weibull distribution can be used to describe the probability of failure of a brittle structure, generalized to a multiaxial case by integrating an equivalent stress (σ_e) over the volume:

$$F = 1 - exp\left(-\frac{1}{V_0}\int\left(\frac{\sigma_e}{\sigma_0}\right)^m dV\right) \qquad (7)$$

Where m is the Weibull modulus, V_0 is a reference volume and σ_0 is the characteristic strength for V_0. The principle of independent action (PIA) is widely used as equivalent stress and account for the action of all the principal stresses independently [33]:

$$\sigma_e = (\sigma_1^m + \sigma_2^m + \sigma_3^m)^{1/m} \qquad (8)$$

In the case of alumina, the values of m, V_0 and σ_0 have been taken from [34]. The estimated probability of failure in the ceramic box is under $2 \cdot 10^{-8}$ in most of the model. The peak value, which occurs near the intersection of the toroidal stiffening wall and one of the radial walls, is as low as $1.63 \cdot 10^{-7}$. This result demonstrates the efficacy of uncoupling as far as possible the thermal expansion of both the ceramic box and the steel case. However, as mentioned in Subsection 2.5, it is not feasible to entrust the response of the supporting system to the difficult prediction of the whole segment (or even sector) deformed shape. Thus, it is preferable to continue developing the promising option 3 of Subsection 2.5 (hinged support + roller support) as interface/supporting system.

7. Pressurization of the ceramic box in case of in-box LOCA

The inert gas which fills the gap between the ceramic box and the steel case should allow detecting and then relieving the overpressure produced by the accidental break of the FW cooling channels. But high pressure zones could appear on the ceramic surface in short transients before detection. For that reason, 2D and 3D CFD transient analyses have been performed in ANSYS Fluent to simulate the pressure evolution at the surface of the wall opposite to the channel break, considering this as an entry with rectangular cross-section (Fig. 10). It has been assumed that the gap is filled with He initially static and at atmospheric pressure. He has been treated as an ideal gas. An inlet pressure of 7.9 MPa has been imposed at the line/surface representing the break, which is parallel to the ceramic surface. The outlet (null gauge pressure) has been located far enough from the inlet to avoid influence on the results during the short temporal range of interest. K-ε with standard wall functions has been selected as turbulence model. The results commented below correspond in general to the 2D model, since their visualization is clearer. The model has been solved for three different values of gap thickness (5, 7.5 and 10 mm). Additionally, six different values of break width (from 2 to 15 mm) have been assessed with a fixed gap thickness of 10 mm.

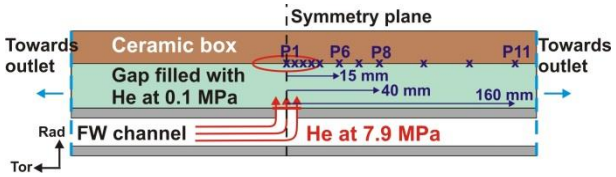

Fig. 10. 2D scheme of the channel break model.

Fig. 11 (bottom) displays the pressure and velocity fields around the break zone at the instant when pressure is the maximum for the case with gap thickness and break width of 10 mm. It can be appreciated how He compressibility prevents the total pressurization of the gap at ~8 MPa. Supersonic pressure waves (>4000 m/s) are generated at the boundary and reach the opposite wall, producing peak pressures around 3.6 MPa. It is a very concentrated load, as also shows the 3D model in a later instant (Fig. 11 top), which rapidly decreases. After $5 \cdot 10^{-5}$ s and until the end of the simulation ($3 \cdot 10^{-4}$ s) the pressure at the surface of the ceramic wall is stabilized at values <2.2 MPa (Fig. 12).

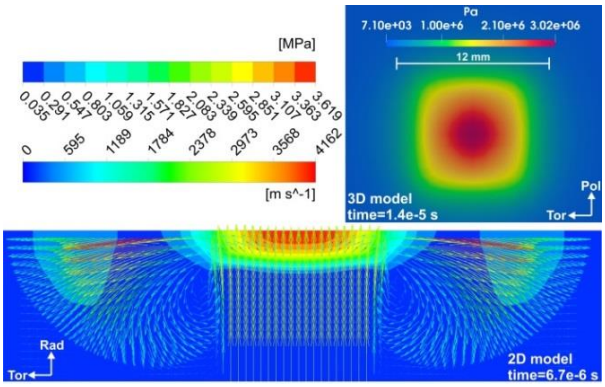

Fig. 11. Bottom: pressure and velocity at $t=6.7 \cdot 10^{-6}$ s (2D model). Top: pressure contours at $t=1.4 \cdot 10^{-5}$ s (3D model). Case with 10 mm gap thickness and 10 mm break width.

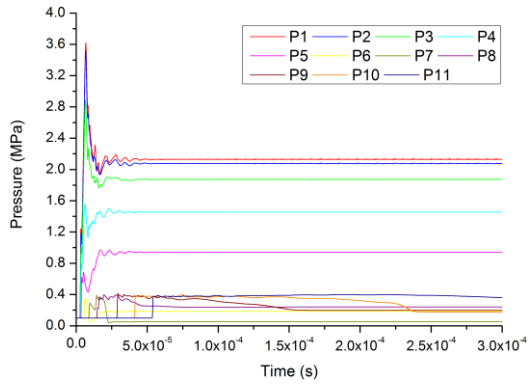

Fig. 12. Pressure transient in several points of the ceramic surface (positions indicated in Fig. 10).

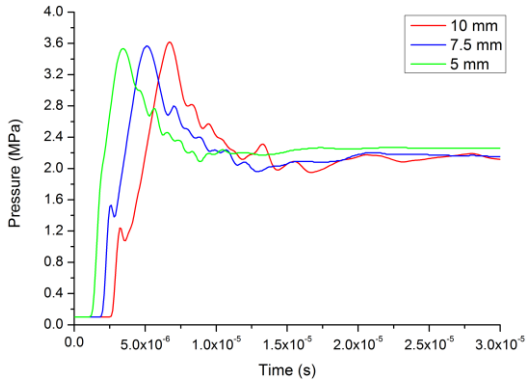

Fig. 13. Comparison of pressure transient in P1 for different gap thicknesses (break width of 10 mm).

Fig. 13 compares the pressure measured at P1 for different gap thicknesses. The three curves are fairly similar, showing a phase difference due to the different travelled distances. It is worth noting that the peak pressure slightly decreases when the gap thickness is reduced, whereas the "background" value is moderately increased. If the gap thickness is fixed in 10 mm and the break size is progressively decreased, two different phenomena are observed. For the range between 15 and 7.5 mm of break width, the pressure curves are similar to the ones shown in Fig. 13. The smaller the break is, the lower the peak value. However, below 7.5 mm successive peaks appear which can exceed the first ones and even the corresponding to bigger break sizes. This is a consequence of the large zone of relatively high pressure formed in front of P1 in the case of the bigger break sizes. It deflects the high velocity streamlines far from the ceramic wall and prevents the re-pressurization of that area over the background value.

These interesting results suggest that the consequences of a He channel break on the structural integrity of the ceramic box can be certainly less important than initially foreseen. Furthermore, they open the door to resize the thickness of the walls and gap, which can be beneficial for the TBR. Nevertheless, the dynamic amplification and especially the brittle behaviour of ceramics should not be forgotten.

8. Tritium breeding and shielding capability

8.1 Tritium breeding performance

One of the main concerns of this design is the impact of the double wall (steel-ceramic) on tritium self-sufficiency. Hence, a heterogenized neutronic model with SiC as material for the ceramic box has been created, given the results of the radiological assessment commented in Subsection 2.1. The model has been prepared using the tool SuperMC MCAM 3.2 [35]. The particle transport calculations have been performed with MCNP5, using the JEFF 3.2 nuclear data library [36]. The direct simulation results have been normalized to $7.094 \cdot 10^{20}$ n/s source, corresponding to a fusion power of 1998 MW.

Despite the total breeder volume is similar to the one of the MMS, the initially assumed thickness of the

double wall (25 mm FW + 25 mm ceramic front wall) plus the 7.5-10 mm gap severely penalize the blanket tritium production. A tritium breeding ratio (TBR) of 1.02 has been calculated for the preliminary design. This value is 13% lower than the value of 1.173 obtained for the last MMS design [3]. Nevertheless, different alternatives have been evaluated (Table 4). The second column in Table 4 indicates the composition of the gap (void or PbLi) and the ceramic walls (SiC, PbLi, a mixture of both or EUROFER). In case 1, the filling gas has been replaced by PbLi. The resulting TBR (1.07) is 5% higher than the baseline one. Such increment is equivalent to the difference of breeder volume in the two cases. In case 2, SiC has been substituted by void, in order to test the behaviour of the ceramic as reflector (and hence its capability to smooth the neutron flux by scattering back neutrons), which could involve a major impact on the PbLi rear channels. A TBR of 1.12 has been obtained. Case 3, as a combination of cases 1 and 2, has provided a TBR of 1.16, implying that the mixed effect is weaker than the sum of both steps. In cases 4.1 to 4.4 the thickness of the SiC walls has been progressively reduced, whereas the amount of PbLi has been conversely increased. This has been done using different proportions of both materials in the homogenized composition of the ceramic box component, which has involved an increase in TBR from 1.09 to 1.15. In the last of them (4.4), the extreme situation in which the ceramic walls have been completely replaced by PbLi, a value of 1.24 has been achieved. Case 5 reflects a situation more similar to the previous MMS designs, with just a structure made of EUROFER, although without internal stiffening plates. The obtained TBR (1.26) is indeed a very high value in comparison with the MMS one (1.173). Finally, case 6 has consisted in the substitution of SiC by EUROFER in the baseline model, in order to provide a second proof of the behaviour of SiC as reflector. Taking into account the achieved TBR (1.05 vs 1.02 in the baseline), it is clear that the depleted tritium breeding performance of the current SMS design compared with the MMS is mainly due to the use of a double wall and the resulting loss of breeder volume, rather than the characteristics of the adopted material (SiC or EUROFER).

In conclusion, the three tested configurations with reduced SiC box thickness (4.1 to 4.3) are promising options that should be further explored.

Table 4. TBR obtained for different configurations.

Cases	Material Gap_Ceramic (0=void)	TBR
Baseline	0_SiC	1.02
1	PbLi_SiC	1.07
2	0_0	1.12
3	PbLi_0	1.16
4.1	0_28%PbLi72%SiC (18 mm walls)	1.09
4.2	0_40%PbLi60%SiC (15 mm walls)	1.12
4.3	0_50%PbLi50%SiC (12.5 mm walls)	1.15
4.4	0_PbLi (no walls)	1.24
5	PbLi_PbLi	1.26
6	0_EUROFER	1.05

8.2 Shielding performance

The SMS design shows a good behaviour in terms of shielding. Nuclear heating in the winding pack (WP) of the toroidal field coils (TFC) is below the quench limit ($5 \cdot 10^{-5}$ W/cm^3) [37] in both the baseline and a configuration with reduced amount of SiC (Fig. 14). Neutron fluence after six full-power years (FPY) in the TFC WP is two orders of magnitude lower than the limit of 10^{18} n/cm^2 [37]. Additionally, both the vacuum vessel and the TFC are well protected against radiation damage (limits of 2.75 and 10^{-4} dpa, respectively [38] [37]) (Fig. 15). The lower port region is an exception due to high streaming in the opening, where including a shielding plug is needed.

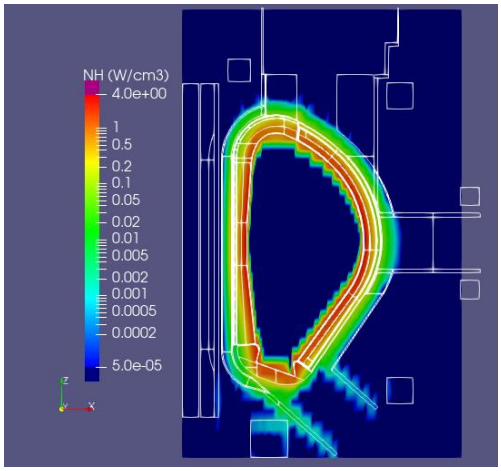

Fig. 14. Mesh tally 3D distribution of nuclear heating (W/cm3) with scale focused on the fulfilment of the TFC quench limit.

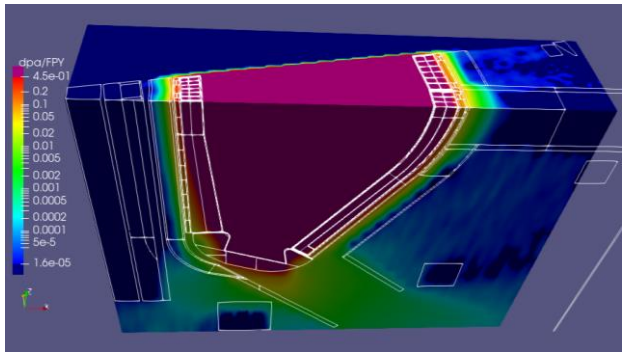

Fig. 15. General 3D map of dpa/FPY in austenitic steel.

9. Conclusions

Different alternatives to upgrade the EU DCLL MMS design to a SMS architecture have been evaluated. It has been proposed to use an electrically resistive and PbLi-compatible ceramic as structural material for the breeding zone, which allows doing without the FCIs and suppresses the limit in the operational temperature imposed by creep in the case of reduced activation steels. The breeding zone is enclosed by a RAFM steel envelope which includes a continuous FW panel cooled

by He. CO_2 has been demonstrated to be a fairly good alternative to He, although possible radiological problems must be clarified.

One of the most critical issues of this concept is the arrangement of the interfaces between the ceramic box and the steel case. The preliminary analyses of two proposed supporting systems point out towards the mechanical feasibility of the design.

The results of the neutronic model using SiC as ceramic material show that the preliminary thickness of the double wall plus the gap compromises the tritium self-sufficiency. However, different variants for the arrangement of the double wall are promising to obtain a suitable TBR. Such variants are supported by the results of CFD models which show that no complete pressurization of the gap occurs if a He channel breaks inwards. In addition to this, the baseline has demonstrated to provide a proper shielding performance.

Acknowledgements

This work has been carried out within the framework of the EUROfusion Consortium and has received funding from the Euratom research and training programme 2014-2018 and 2019-2020 under grant agreement No 633053. The views and opinions expressed herein do not necessarily reflect those of the European Commission. This work has been partially supported by the computing facilities of Extremadura Research Centre for Advanced Technologies (CETA-CIEMAT), funded by the European Regional Development Fund (ERDF). CETA-CIEMAT belongs to CIEMAT and the Government of Spain.

References

[1] D. Rapisarda et al. “Conceptual design of the EU-DEMO dual coolant lithium lead equatorial module”, IEEE Trans. Plasma Sci. 44 (2016) 1603-1612.

[2] I. Fernández-Berceruelo et al., “Thermal-hydraulic design of a DCLL breeding blanket for the EU DEMO”, Fusion Eng. Des. 124 (2017) 822-826.

[3] I. Fernández-Berceruelo et al., “Remarks on the performance of the EU DCLL breeding blanket adapted to DEMO 2017”, Fusion Eng. Des. 155 (2020) 111559.

[4] N.P. Taylor et al., “A model of the availability of a fusion power plant”, Fusion Eng. Des. 51-52 (2000) 363-369.

[5] W.E. Han, D.J. Ward, “Revised assessments of the economics of fusion power”, Fusion Eng. Des. 84 (2009) 895-898.

[6] R. Lindau et al., “Present development status of EUROFER and ODS-EUROFER for application in blanket concepts”, Fusion Eng. Des. 75-59 (2005) 989-996.

[7] G. Pintsuk et al., “European materials development: results and perspective”, Fusion Eng. Des. 146 (2019) 1300-1307.

[8] D. Iadicicco et al., “Multifunctional nanoceramic coatings for future generation nuclear systems”, Fusion Eng. Des. 146 (2019) 1628-1632.

[9] M.S. Tillack et al., “Fusion power core engineering for the ARIES-ST power plant”, Fusion Eng. Des. 65 (2003) 215-261.

[10] F.R. Urgorri et al. “Magnetohydrodynamic and thermal analysis of PbLi flows in poloidal channels with flow channel insert for the EU-DCLL blanket”, Nucl. Fusion 58 106001, 2018.

[11] I. Fernández-Berceruelo et al., “Large-scale behavior of sandwich-like FCI components within the EU-DCLL operational conditions”, Fusion Eng. Des. 136 (2018) 633-638.

[12] X-5 Monte Carlo Team, “MCNP – a general Monte Carlo n-particle transport code version 5”, 2017.

[13] The JEFF-3.1.1 OECD, NEA No 6807, 2009.

[14] J. Sanz et al., NEA Data Bank (NEA-1839), 2009.

[15] R.A. Forrest et al., UKAEA FUS pp. 535, 2007.

[16] S. Wang et al., “Comparative analysis of the efficiency of a CO_2-cooled and a He-cooled pebble bed breeding blanket for the EU DEMO fusion reactor”, Fusion Eng. Des. 138 (2019) 32-40.

[17] Y. Wu and the FDS Team, “Design status and development strategy of China liquid lithium-lead blankets and related material technology”, Journal of Nucl. Mat. 367-370 (2007) 1410-1415.

[18] DEMO1 PROCESS output (May 3rd 2017), EFDA_D_2NDSKT.

[19] C. Mistrangelo et al., “Three-dimensional magneto convective flows in geometries relevant for DCLL blankets”, Fusion Eng. Des. 159 (2020) 11686.

[20] L. Moya et al., “Structural assessment of a DCLL SMS - 2020”, presentation for EUROfusion task BB-4.2.1-T008-D002, 2020.

[21] F. Maviglia et al., “Optimization of DEMO geometry and disruption location prediction”, Fusion Eng. Des. 146 (2019) 967-971.

[22] V. Gnielinski, “New equations for heat and mass transfer in the turbulent pipe and channel flow”, Int. Chem. Eng. 16 (1976) 359-368.

[23] F. Gillemot et al., Material Property Handbook: pilot project on EUROFER97, EFDA_D_2MT9X8, 2016.

[24] NIST thermophysical properties of fluid systems, https://webbook.nist.gov/chemistry/fluid.

[25] W. Davis et al., ITER Material Properties Handbook. Material: pure tungsten. Property: thermal conductivity. ITER_D_2237RQv1.0.

[26] J.I. Linares et al., Supercritical CO2 Brayton power cycles for DEMO fusion reactor based on Helium Cooled Lithium Lead blanket, Appl. Therm. Eng. 76 (2015) 123-133.

[27] T.Q. Hua and J.S. Walker, “MHD considerations for poloidal-toroidal coolant ducts of self-cooled blankets”, Fusion Technol. 19 (1991) 951-960.

[28] J.A. Shercliff, “Steady motion of conducting fluids in pipes under transverse magnetic fields”, Math. Proc. Cambridge Philos. Soc. 49 (1) 136144, 1953.

[29] R. Stieglitz et al., “Magnetohydrodynamic flow in a right-angle bend in a strong magnetic field”, J. Fluid Mech. 326 (1996) 91-123.
[30] D. Martelli et al., “Literature review of lead-lithium thermophysical properties”, Fusion Eng. Des 138 (2019) 183-195.
[31] “High purity 99.9% alumina material specifications”, https://www.technicalproductsinc.com.
[32] L. Moya et al., “Structural assessment of a DCLL SMS - 2019”, EUROfusion report, EFDA_D_2N9FF9, 2019.
[33] R. Bermejo, R. Danzer, “Mechanical characterization of ceramics: designing with brittle materials”, Comprehensive hard materials 2 (2014) 285-298.
[34] G. Quinn, “Flexure strength of advanced ceramics – a round robin exercise”, U.S. Army Materials Technology Laboratory, 1989.
[35] Y. Wu and the FDS Team, “CAD-based interface programs for fusion neutron transport simulation”, Fusion Eng. Des. 84 (2009) 1987-1992.
[36] The JEFF-3.2 Nuclear Data Library, NUCLEAR ENERGY AGENCY, OECD.
[37] J.L. Duchateau et al., “Conceptual design for the superconducting magnet system of a pulsed DEMO reactor”, Fusion Eng. Des. 88 (2013) 1609-1612.
[38] C. Bachmann, “DEMO plant requirements document”, EFDA_D_2MG7RD_v1.8, 2014.